Journal of Materials Chemistry C

ROYAL SOCIETY OF CHEMISTRY

PAPER

View Article Online
View Journal

Cite this: DOI: 10.1039/d0tc05669c

High-performance perovskite light-emitting diodes based on double hole transport layers†

Weigao Wang,[ab] Zhenghui Wu,[b] Taikang Ye,[b] Shihao Ding,[b] Kai Wang,[bc] Zhengchun Peng *[a] and Xiao Wei Sun*[bc]

Received 2nd December 2020,
Accepted 28th December 2020

DOI: 10.1039/d0tc05669c

rsc.li/materials-c

Preparing perovskite light emitting diodes (PeLEDs) by a solution process leads to inevitable imbalanced carrier injection and solvent erosion, which prevent us from obtaining high-performance PeLEDs. Here, we report a facile method to fabricate green-emitting PeLEDs with double hole transport layers (HTLs) that significantly promote the hole injection and charge balance. To address the problem of solvent erosion, 1,4-dioxane was adopted as the solvent for poly(9-vinylcarbazole) (PVK) and it was cast onto the surface of poly[(9,9-dioctylfluorenyl-2,7-diyl)-*co*-(4,40-(*N*-(*p*-butylphenyl))-diphenylamine)] (TFB). At the same time, an orthogonal solvent 1,4-dioxane was employed to improve the surface smoothness of the perovskite film on the double HTLs. The PeLEDs with TFB/PVK double HTLs showed a maximum current efficiency (CE) and an EQE of 53.5 cd A^{-1} and 12.9%, respectively. The EQE of the device is about 1.7 and 3 times higher than that of the single HTL device with PVK and TFB, respectively. This remarkable improvement is mainly attributed to the cascade-like energy alignment of the double HTLs, which prevents charging in perovskite nanocrystals (NCs). This work offers a new insight into preparing high performance PeLEDs for displays and lighting devices.

Introduction

Solution-processed metal halide perovskite nanocrystals (NCs) exhibit significant potential for applications in light-emitting diodes (LEDs) due to their excellent optoelectronic properties such as high charge carrier mobility, high photoluminescence quantum yield (PLQY) and narrow emission line-width.[1–5] So far, various strategies have been devoted to improve the performance of perovskite light emitting diodes (PeLEDs), including surface ligand engineering,[6,7] compositional doping engineering[8–10] and device interface optimization.[11,12] Due to continuous efforts from the research community, the peak external quantum efficiencies (EQEs) have exceeded 20% for both green[13] and red[14] PeLEDs. Nevertheless, PeLEDs still face some challenges that need to be overcome, such as poor stability, imbalance between electron and hole injection and solution erosion during the solution preparation of multilayer structures.

Imbalanced electron and hole injection will lead to deterioration of the device efficiency and the operational stability of PeLEDs. In many green- and blue-emitting PeLEDs with forward structures, the energy levels of the highest occupied molecular orbital (HOMO) of commercial materials for hole transport layers (HTLs) such as poly(*N*,*N*0-bis(4-butylphenyl)*N*,*N*0-bis(phenyl)benzidine) (Poly-TPD; −5.2 eV)[15] and poly[9,9-dioctylfluorene-*co*-*N*-[4-(3-methylpropyl)]-diphenylamine] (TFB; −5.3 eV)[16] are much higher than the valence band maximum (VBM) levels of perovskite emitting layers. This means that it is difficult to inject holes into the emission layer due to the large energy barrier between the HTL and the perovskite layer. In contrast, the electron is easily injected into the perovskite NC layer because there is little energy barrier between the electron transport layer (ETL) (*e.g.* 2′,2′-(1,3,5-benzinetriyl)-tris(1-phenyl-1-*H*-benzimidazole) (TPBi)) and the perovskite layer.[12,17] Excessive electron injection causes imbalanced carrier injection of devices, which could charge the exciton state of NCs, and thus lead to enhanced nonradiative auger recombination and a high turn-on voltage.[18] In order to balance the injection of carriers, researchers have adopted a variety of strategies. They are mainly divided into two categories, *i.e.*, blocking electron injection and enhancing hole injection. The use of some functional layers such as polyvinyl pyrrolidine (PVP),[19] poly[(9,9-bis(30-(*N*,*N*-dimethylamino)propyl)-2,7-fluorene)-*alt*-2,7-(9,9-ioctylfluorene)] (PFN),[17] ZnMgO[20] and

[a] *Key Laboratory of Optoelectronic Devices and Systems of Ministry of Education and Guangdong Province, College of Physics and Optoelectronic Engineering, Shenzhen University, Shenzhen, Guangdong, 518060, P. R. China. E-mail: zcpeng@szu.edu.cn*

[b] *Guangdong University Key Lab for Advanced Quantum Dot Displays and Lighting, Shenzhen Key Laboratory for Advanced Quantum Dot Displays and Lighting, and Department of Electrical and Electronic Engineering, Southern University of Science and Technology, Shenzhen 518055, China. E-mail: sunxw@sustech.edu.cn*

[c] *Key Laboratory of Energy Conversion and Storage Technologies (Southern University of Science and Technology), Ministry of Education, Shenzhen 518055, China*

† Electronic supplementary information (ESI) available. See DOI: 10.1039/d0tc05669c

polyethylenimine (PEI)[21] can significantly block electron injection to achieve balanced carrier recombination and enhance the performance of devices. Another method is to build a cascade-like energy alignment by double HTLs, so that the hole injection is improved. Dai employed solution-processed poly-TPD/poly(9-vinylcarbazole) (PVK) bilayer structures to adjust the energy level alignments in HTLs. As a result, the preparation of CdSe/CdS QD-LEDs exhibited high saturation deep-red emission and a high external quantum efficiency (EQE) of up to 20.5%.[22] Also, the bilayer structure was reported to improve the hole transport and injection in high-performance blue CdSe/ZnS QD-LEDs, which was due to the advantages of the deep HOMO level of PVK (~ -5.8 eV) and the cascade-like energy alignment with the poly-TPD/PVK layer.[15] Some researchers also used TFB instead of poly-TPD as a double hole injection layer of TFB/PVK to improve the hole injection and performance of optoelectronic devices, because TFB has a higher hole mobility ($\sim 1 \times 10^{-2}$ cm^2 V^{-1} s^{-1})[23] and a deeper HOMO level than poly-TPD ($\sim 1 \times 10^{-4}$ cm^2 V^{-1} s^{-1}; ~ -5.2 eV).[24] Double HTLs can facilitate hole injection in QD-LEDs with cascade-like energy alignment. However, there are only a few studies in which double HTLs were utilized to improve the performance of PeLEDs. Wu and Li chose chlorobenzene (CB) and toluene as the solvents for TFB and PVK to fabricate bilayer HTLs to realize efficient hole injection in PeLEDs.[25,26] Zou applied a poly-TPD/PVK bilayer to balance the electron and hole transport, which were processed from CB solutions.[27] The bilayer HTL, combined with sapphire substrates, resulted in the suppression of efficiency roll-off at high current densities in PeLEDs. However, in practice, the morphology of a TFB/PVK or poly-TPD/PVK bilayer was difficult to control and repeat if both TFB and PVK (or poly-TPD and PVK) were dissolved in the same organic solvent. To improve the process window, orthogonal solvents for TFB/PVK or the poly-TPD/PVK bilayer are necessary. Liu employed CB and an orthogonal solvent *m*-xylene to dissolve PVK and TFB, respectively. Then the TFB/PVK double-layer was spin-cast as an HTL, which improved the hole injection in blue perovskite devices.[28] However, the solubility of TFB in *m*-xylene is sensitive to temperature, which affected the morphology of the film. A suitable solvent for PVK is needed to eliminate the erosion of the underlying TFB layer, so that the double HTLs can fully realize their advantages in improving the hole injection and the electroluminescence (EL) performance of the devices.

Herein, we employ an orthogonal solvent of 1,4-dioxane for PVK and CB for TFB to prepare double HTLs, which can effectively eliminate the solvent erosion in HTLs and ensure a uniform morphology for the perovskite film on top. The TFB/PVK double HTL not only improved the hole injection with cascade-like energy alignment, but also was important for achieving a smooth morphology and excellent emission of perovskite thin films. In consequence, the PeLEDs exhibited a low turn-on voltage of 2.9 V, a maximum current efficiency (CE) of 53.5 cd A^{-1} and a peak of external quantum efficiency (EQE) of 12.9%. The EQE was about 1.7 and 3 times higher than that of the device with single-layer PVK and TFB as HTLs, respectively. Our work provides an effective approach to fabricate efficient and stable PeLEDs.

Results and discussion

In solution-processed PeLEDs, the choice of solvent is very important, since it significantly influences the morphology of the thin films, and thus the device performances. To fabricate TFB/PVK double HTLs, CB was fixed as the solvent for TFB, while 1,2-dichlorobenzene, toluene, *m*-xylene and 1,4-dioxane were used as the solvents for PVK to explore the effect of solvent erosion on the TFB layer. To explore the impact of the four solvents on the TFB layer, we used the spin-coating method to prepare indium tin oxide (ITO)/poly(3,4-ethylenedioxythiophene) poly(styrenesulfonate) (PEDOT:PSS)/TFB multilayers. In the solvent rinsing experiment, 100 μl of different solvents (1,2-dichlorobenzene, toluene, *m*-xylene and 1,4-dioxane, respectively) were spin-coated onto the TFB layer at a speed of 4000 rpm for 45 s. Then the steady-state PL of the washed TFB layers was measured for evaluating the effects of various solvents. The changes with respect to the pristine TFB layer were compared to reflect the impact of solvent erosion. Fig. 1 shows the PL intensities of the TFB layers rinsed with various solvents. It can be seen that the solvents 1,2-dichlorobenzene (Film 1), toluene (Film 2) and *m*-xylene (Film 3) result in a drastic decrease in the intensity, indicating severe erosion on the underlying TFB layer. However, the PL intensity of the TFB film rinsed with 1,4-dioxane (Film 4) is only slightly decreased compared to that of the pristine film (Film 5), suggesting that the TFB layer had excellent resistance to corrosion of the polar solvent 1,4-dioxane. The result also illustrates that the orthogonal solvent 1,4-dioxane selected can effectively avoid solvent erosion. The film thicknesses of the PEDOT:PSS/TFB multilayers after rinsing with 1,2-dichlorobenzene, toluene, *m*-xylene, and 1,4-dioxane and of the pristine films were around 48 nm, 52 nm, 58 nm, 78 nm and 84 nm, respectively, which also indicates that 1,4-dioxane showed minimum erosion on the TFB layer.

The morphology of the film is important for the performance of the device.[12,29] Therefore, atomic force microscopy (AFM) was utilized to investigate the surface morphology of the ITO glass substrate/PEDOT:PSS/TFB multilayers with and without being rinsed with various solvents, as shown in Fig. 2.

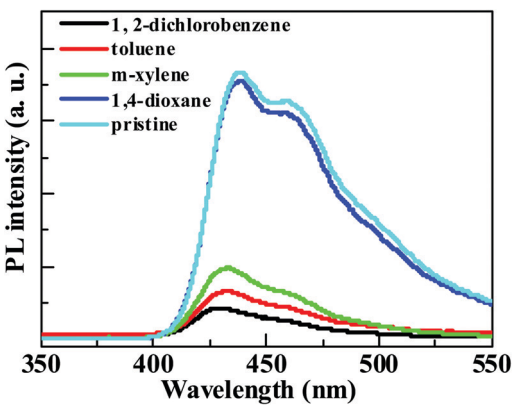

Fig. 1 PL spectra of ITO/PEDOT:PSS/TFB films w/o rinsing with various solvents. Film 1: 1,2-dichlorobenzene; film 2: toluene; film 3: *m*-xylene; film 4: 1,4-dioxane; film 5: pristine.

Compared to the pristine TFB film, the root mean square (RMS) roughness of the TFB films significantly increased after being rinsed with 1,2-dichlorobenzene and toluene. However, the RMS roughness of the TFB film rinsed with *m*-xylene and 1,4-dioxane only slightly increases. This suggested that *m*-xylene and 1,4-dioxane cause little solvent erosion on the underlying TFB layer.

In addition, different solvents for PVK also make significant differences on the morphologies of the double HTLs. The AFM images shown in Fig. 3 exhibit the surface morphologies of the ITO/PEDOT:PSS/TFB/PVK multilayers with the PVK overlayer spin-cast from (a) 1,2-dichlorobenzene, (b) toluene, (c) *m*-xylene, and (d) 1,4-dioxane. When 1,2-dichlorobenzene and toluene were used as the solvents for PVK, there were a large number of isolated islands on the surface of the film observed and the RMS roughness greatly increased to 3.1 nm and 4.7 nm (Fig. 3a and b). This was because 1,2-dichlorobenzene and toluene caused serious erosion on the underlying TFB layers, consistent with Fig. 2. On the other hand, the AFM image of PVK thin films cast from 1,4-dioxane solution (Fig. 3d) exhibited a flat, continuous surface with a RMS roughness of 0.8 nm. The formation of TFB/PVK double HTLs with a better surface morphology was due to the less solvent erosion on the TFB layer with 1,4-dioxane. As an interface modification layer to improve the surface morphology and the interface properties in the devices, it was reported that the PVK layer can effectively suppress non-radiative recombination.[17] Since the solubility of PVK in *m*-xylene is very sensitive to temperature,[29] the PVK solution needs to be stored above 50 °C. When hot PVK solution was spin-coated onto the substrate at room temperature, PVK quickly formed precipitates and induced irregular bulges on the substrate, resulting in an increased RMS roughness (1.6 nm shown in Fig. 3c).

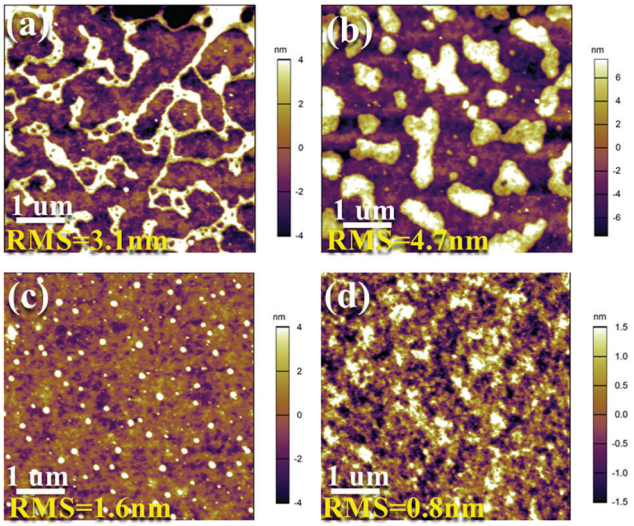

Fig. 3 AFM images of ITO/PEDOT:PSS/TFB/PVK multilayers with PVK overlayers spin-cast from (a) 1,2-dichlorobenzene, (b) toluene, (c) *m*-xylene, and (d) 1,4-dioxane.

In order to verify the rationality of applying the double HTLs, green PeLEDs with the device architecture of ITO/PEDOT:PSS (45 nm)/TFB (40 m)/PVK (8 nm)/$FAPb_{0.7}Sn_{0.3}Br_3$ NCs (40 nm)/1,3,5-tris(1-phenyl-1*H*-benzimidazol-2-yl)benzene (TPBi, 40 nm)/lithium fluoride (LiF, 1 nm)/Al (100 nm) were fabricated, as

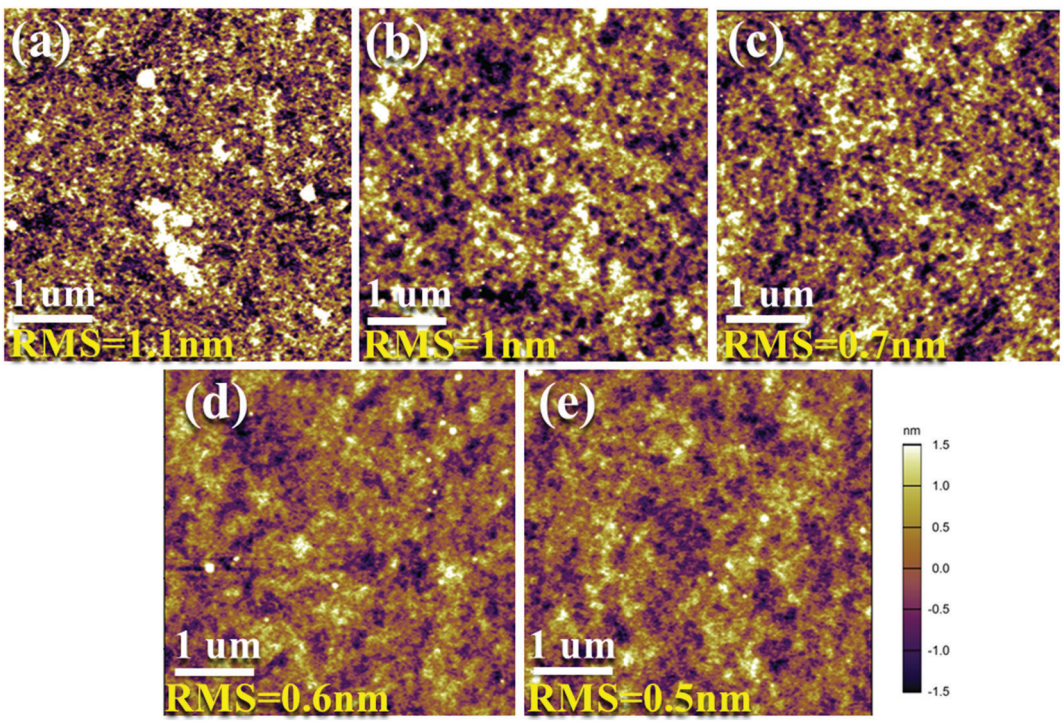

Fig. 2 AFM images of ITO/PEDOT:PSS/TFB multilayers with and without being rinsed with various solvents: (a) 1,2-dichlorobenzene, (b) toluene, (c) *m*-xylene, and (d) 1,4-dioxane, and (e) the pristine.

shown in Fig. 4a. In this device, PEDOT:PSS was used as hole injection layers (HILs), the TFB and PVK layers as double HTLs, $FAPb_{0.7}Sn_{0.3}Br_3$ NCs as the emitting layer and the TPBi film as the electron-transport layer (ETL). The corresponding cross-sectional scanning electron microscopy (SEM) images of the devices based on TFB/PVK double HTLs are shown in Fig. S1a (ESI†). The boundary of the multiple layers could be clearly observed, and all the functional layers were not inter-affected by each other after spin-coating. The normalized UV-Vis absorption spectrum and PL spectrum of the $FAPb_{0.7}Sn_{0.3}Br_3$ NCs are shown in Fig. S1b (ESI†), and the PL peak position of these NCs located at 523 nm showed a full width at half maximum (FWHM) of ~23 nm. Fig. 4b shows the energy level diagram of the functional layers in the PeLED devices. The energy levels were taken from ref. 30–32. The high conduction band minimum (CBM) of the TPBi ETL allows for efficient electron injection into the NC emission layer, since the electron injection barrier from the ETL to the NC emitting layer was very small. There was an energy gap of 0.5 eV between the HOMO of the TFB HTL and the VBM of NCs, while the energy gap between the PVK HTL and PEDOT:PSS was also very large (as seen in Fig. 4b). Therefore, the electrons dominate charge injection into NC perovskite devices, and the holes are minority charges in the PeLEDs due to the less efficient hole injection.[19,21] Enhancing the hole injection rate is expected to improve the charge balance. Here, we reduced this large hole injection barrier by coating a thin layer (~8 nm) of PVK on top of the TFB film to form a double HTL. The bilayer structure helps to reduce the hole injection barrier, promote the hole injection, and improve the balance of injected carriers, thus improving the electroluminescence efficiency of the device.

The PVK layer also played another important role in preparing high-efficiency PeLEDs, since it can suppress charging of the perovskite NCs, and maintaining the superior emission performance of the perovskite film.[11] In order to further investigate the photoinduced excitations within the perovskite NC films on different HTL layers, the time resolved (TR) PL of the perovskite NC films on different HTL layers was measured (Fig. 4c). The calculated average PL lifetime (Table S1, ESI†) of the $FAPb_{0.7}Sn_{0.3}Br_3$ films dramatically decreased from 61 ns to 2.7 ns, if the glass/ITO substrate was replaced by a glass/ITO/PEDOT:PSS/TFB substrate, which was consistent with the dramatic reduction in photoluminescence (as seen in Fig. 4d). According to previous research,[33–35] this dramatic change was caused by the non-radiative recombination; such a non-radiative channel is generated through the defect states in the TFB or *via* a charge transfer process. The average PL lifetime of perovskite films on the double HTLs greatly increased to ~11.3 ns, and PL intensity also increased (Fig. 4d). Both the increased PL lifetime and PL intensity suggest that the PVK layer reduces the exciton quenching by separating the perovskite film from the TFB layer. The average PL lifetime of ~49 ns (Fig. 4c) and the significantly improved PL intensity of the

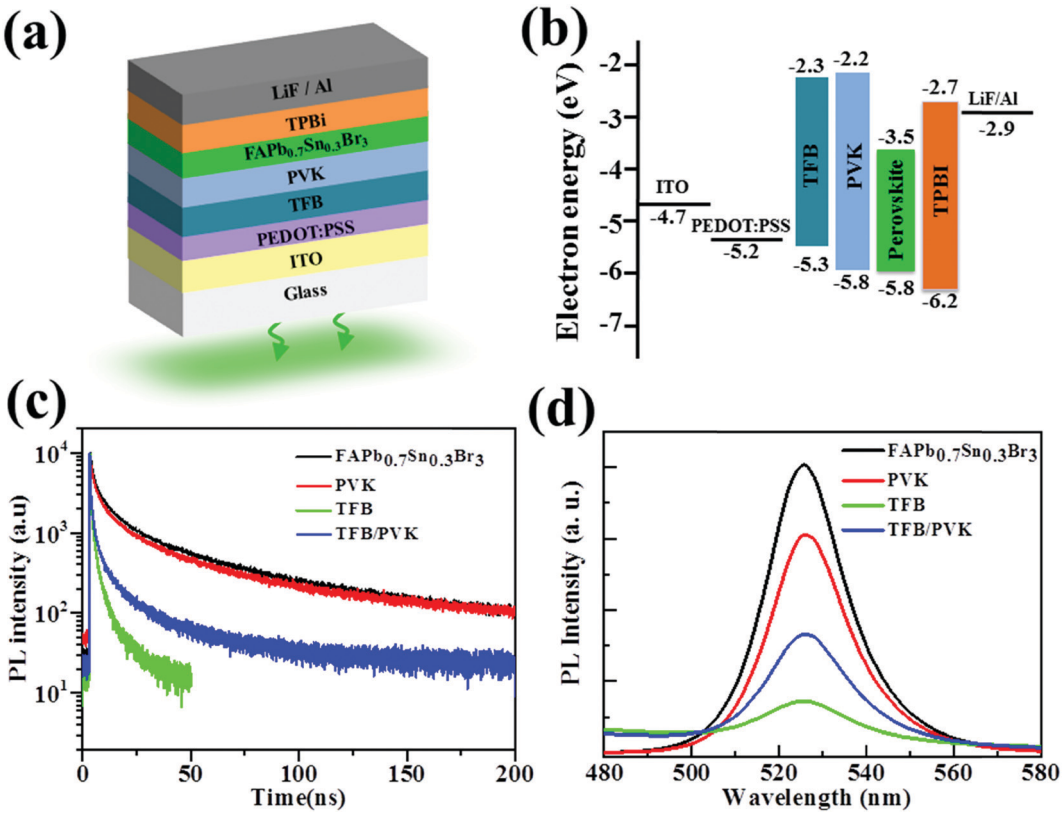

Fig. 4 (a) Device configuration and (b) the energy level diagram for each layer in the PLED structure. (c) TRPL decay curves and (d) PL intensities of the $FAPb_{0.7}Sn_{0.3}Br_3$ films cast on top of glass, PVK, TFB and TFB/PVK, respectively.

perovskite thin films on the pristine PVK layer (Fig. 4d) also indicate that the PVK layer reduced the non-radiative recombination pathways. The PVK layer in the double HTL improved the PL intensities of the perovskite films, which is beneficial for fabricating high-efficiency PeLEDs.

To investigate the impact of the solvent for PVK on the device performance, we fabricated PeLEDs based on TFB/PVK double HTLs with a PVK interlayer spin-cast from different solvents. The current density (J)–voltage (V)–luminance (L) characteristics of the PeLEDs with the PVK layer spin-cast from 1,2-dichlorobenzene, toluene, *m*-xylene, and 1,4-dioxane are shown in Fig. 5a. These devices exhibited a low turn-on voltage of 3 V, which was due to the efficient hole injection from the TFB/PVK double HTLs with cascade-like energy level alignment.[25,26] The current density of the device with PVK (in 1,4-dioxane) was the lowest at the low voltage, which indicated the smallest leakage current of the device. This was also consistent with the film morphology measurement as shown in Fig. 1 and 2. Therefore, the EQE for the control devices with PVK interlayers spin-cast from 1,2-dichlorobenzene, toluene and *m*-xylene showed lower performance with 3.4%, 4.5% and 5.4%, respectively (Fig. 5b). On the other hand, the device with the PVK interlayer spin-cast from 1,4-dioxane showed an EQE of 12.2%, which is 72%, 63% and 55% higher than those of the other three control devices. Therefore, the poor surface morphology for the PVK HTL of the three control devices is possibly the reason for the low performance.

Fig. 6(a) shows the J–V–L characteristics of PeLEDs with single and double HTLs. The current density of PeLEDs with the TFB/PVK double-layer was much higher than those of the control devices based on the single-layer of PVK and TFB as HTLs. The turn-on voltage of ~2.93 V for the devices with TFB/PVK bilayers was much lower than those of the devices with PVK (3.7 V) and TFB (3.05 V) HTLs. In particular, the devices with PVK only as an HTL showed a very low current density at a high voltage, which was due to the low hole mobility of PVK ($\sim 2.5 \times 10^{-6}$ cm^2 V^{-1} s^{-1})[15] and the large energy barrier between PEDOT:PSS and PVK. The TFB/PVK double HTLs with a cascade-like energy level alignment reduce the injection barrier of the hole, hence improving the hole transport and injection and the emission efficiency of the devices.

The device based on TFB/PVK showed the maximum brightness of 10 520 cd m^{-2} at 7.4 V. The peaks of current efficiency (CE) and EQE of the PeLED device with TFB/PVK were 53.5 cd A^{-1} and 12.9% (Fig. 6b and Fig. S2, ESI†), respectively. The EQE is about 1.7 and 3 times higher than those of the control device based on the single-layer of PVK and TFB, respectively. The detailed information about the device performance is summarized in Table S2 (ESI†). To verify the repeatability, the EQE of 16 devices with TFB/PVK from four batches of fabrication was tested. As shown in Fig. S3 (ESI†), the devices showed an average peak EQE of 11.7%, indicating excellent device reproducibility. The EL spectra of the devices with different HTLs showed a peak at 528 nm and a FWHM of ~23 nm, as seen in Fig. 6c. The inset of Fig. 6c shows the photo of a working device (0.04 cm^2) driven at 7 V, demonstrating high color purity with green emission.

To investigate the impacts of different HTLs on the charge injection and transport, the hole-only devices (HODs) ITO/PEDOT:PSS/HTL/$FAPb_{0.7}Sn_{0.3}Br_3$ NCs/4,4,4-tris(*N*-carbazolyl)-triphenylamine (TcTa)/*N*,*N*′-bis(naphthalen-1-yl)-*N*,*N*′-bis(phenyl)-benzidine (NPB)/dipyrazino[2,3-*f*:2′,3′-*h*]quinoxaline-2,3,6,7,10,11-hexacarbonitrile (HATCN)/Al and the electron-only devices (EODs) ITO/ZnMgO/PEI/$FAPb_{0.7}Sn_{0.3}Br_3$ NCs/TPBI/LiF/Al were fabricated. As shown in Fig. 6(d), the hole current density of the HOD with a TFB/PVK double-layer is higher than those of the HODs with a PVK or TFB single HTL, implying that the current density of holes was enhanced by double HTLs. The current density of the EOD is greater than those of the HODs, indicating that electron is the major carrier. However, the current density of the HOD based on the TFB/PVK double-layer was closer to that of the EOD, which explains that the TFB/PVK double-layer structure was beneficial for improving the carrier injection balance and for enhancing the performance of the device.

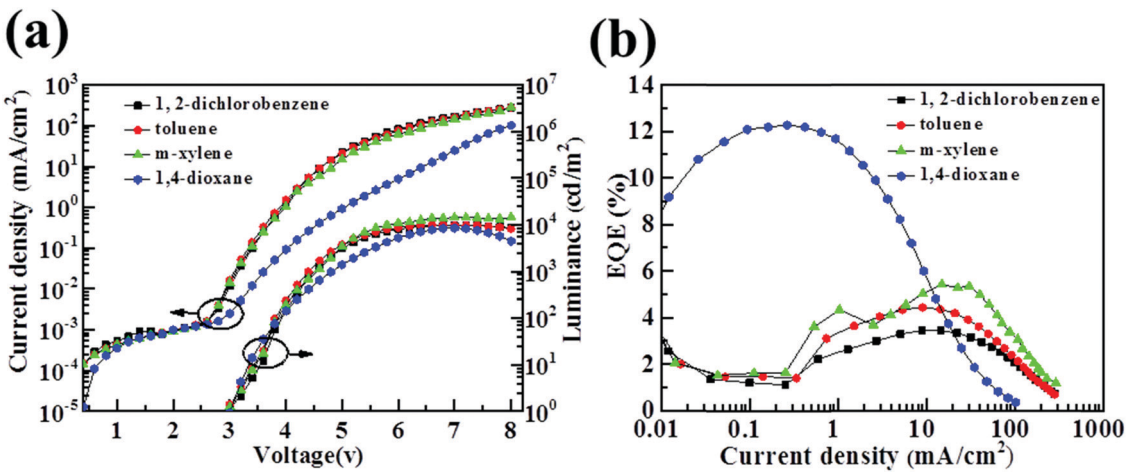

Fig. 5 (a) J–V–L characteristics of the devices. (b) EQE–J characteristics of the PeLEDs with PVK interlayers spin-cast from different solvents.

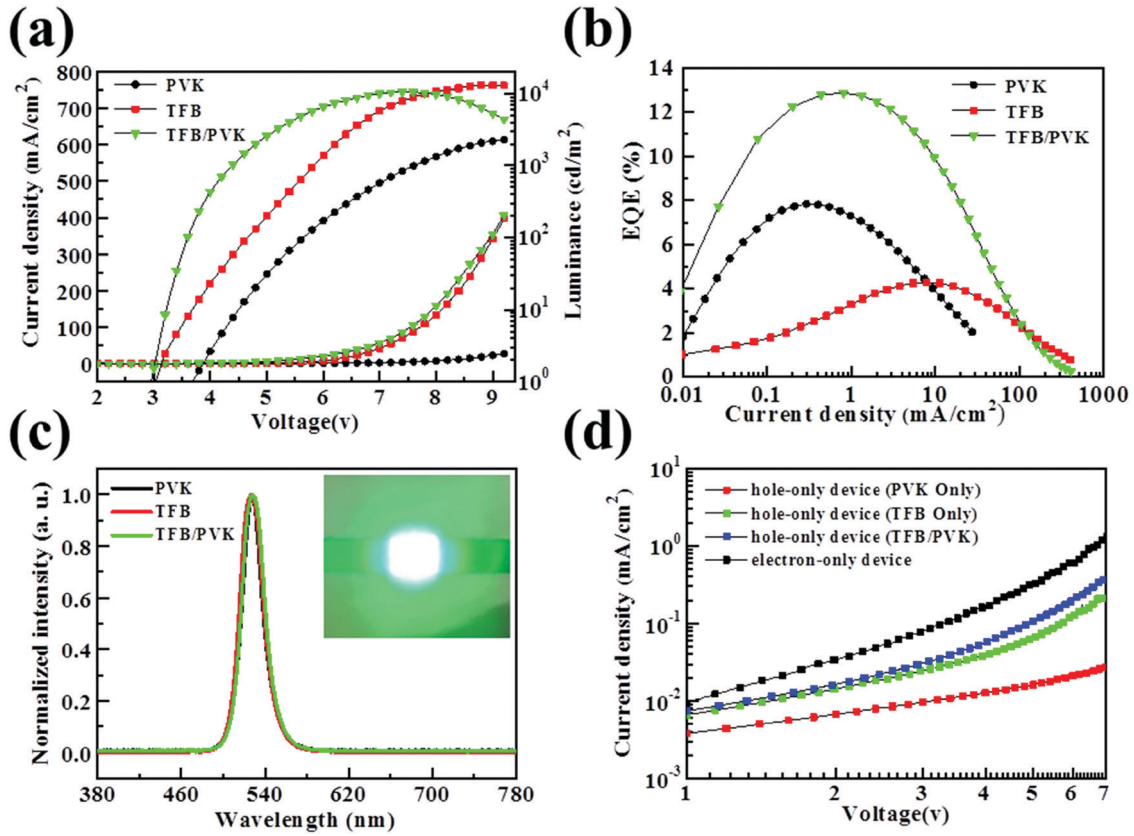

Fig. 6 (a) *J*–*V*–*L* and (b) EQE–*J* characteristics of the PeLEDs based on single and double HTLs. (c) Normalized EL spectra of the devices (inset: photo of the optimal device driven at 7 V). (d) *J*–*V* characteristics of the electron-only device and hole-only devices with PVK, TFB and TFB/PVK HTLs.

Conclusion

In summary, we proposed a facile and simple method utilizing 1,4-dioxane as the solvent for PVK to prepare TFB/PVK double HTLs. By comparative studies, we show that 1,4-dioxane solvent resulted in the best performance, since it avoided solvent erosion of the underlying TFB layers, leading to a pinhole-free TFB/PVK double HTL at room temperature. The devices with a TFB/PVK double-layer exhibited a high current efficiency of 53.5 cd A^{-1} and a peak of external quantum efficiency (EQE) of 12.9%, which accounts for 1.7 and 3 times increase in the EQE compared to the device with only PVK and TFB layers as the HTLs, respectively. This excellent device performance was attributed to the improved hole injection, the suppression of charging in perovskite NCs, and the improved emission efficiency of the perovskite thin films in the devices with TFB/PVK double HTLs. This research will provide an effective approach to improve the performance of PeLEDs.

Experiment

Materials

Lead(II) bromide ($PbBr_2$, powder, 98%), hydrobromic acid (HBr, 48 wt% in H_2O, 99.99%), *N*,*N*-dimethylformamide (C_3H_7NO, anhydrous, 99.8%) and acetonitrile (CH_3CN, anhydrous, 99.8%) were purchased from Sigma-Aldrich. Tin(II) bromine ($SnBr_2$, powder, 99%) was purchased from J&K Scientific. Formamidinium bromine (FABr, powder, 99%) was purchased from Xi'an p-OLED. Methylamine (CH_5N, 30–33 wt% in ethanol), oleylamine ($C_{18}H_{37}N$, 80–90%), oleic acid ($C_{18}H_{34}O_2$), 1,2-dichlorobenzene, *m*-xylene and 1,4-dioxane were purchased from Aladdin. Chloroform, toluene, and hexane were purchased from Shanghai Lingfeng Chemical Reagents.

Synthesis of $FAPb_{1-x}Sn_xBr_3$ NCs

The perovskite nanocrystals ($FAPb_{1-x}Sn_xBr_3$) are synthesized at room temperature in air, following Cai's work.[28] When $x = 0.3$, the performance of the prepared device is the best, so we chose $FAPb_{0.7}Sn_{0.3}Br_3$ as the light-emitting layer to fabricate the device in this work. Firstly, 0.1 mmol of $PbBr_2$ and $SnBr_2$ mixture with different stoichiometric ratios ($PbBr_2$: $SnBr_2$ = $1 - x : x$, x from 0 to 1 with step of 0.1) and 0.1 mmol FABr were dissolved in 1 mL of *N*,*N*-dimethylformamide (DMF) solution. Secondly, 200 μL oleic acid and 40 μL oleyl amine were added to the mixed solution to form a precursor. After thorough mixing of the precursor, 400 μL precursor was added to 10 mL of chloroform, and the mixture solution became a colloid with a yellow green appearance after being slightly stirred. 5 mL of toluene/acetonitrile mixture (volume ratio 1 : 1) was added to the colloidal solution for further purification. At last, the sediment was redisposed into 3 mL of *n*-hexane after centrifuging at 7500 rpm for 4 min.

Device fabrication

Devices with the structure of glass/ITO/PEDOT:PSS (45 nm)/TFB (40 m)/PVK (8 nm)/$FAPb_{0.7}Sn_{0.3}Br_3$ NCs (40 nm)/TPBi (40 nm)/LiF (1 nm)/Al (100 nm) were fabricated. The ITO glasses (sheet resistance = 20 Ω sq^{-1}) were sequentially cleaned with detergent, deionized water, and isopropanol by ultrasonication for 20 min each, followed by treatment in ultraviolet-ozone for 20 min. Then a PEDOT:PSS (Clevios AI 4083) layer was formed by spin-casting at 3000 rpm for 45 s onto the pre-cleaned ITO-substrate, which was then baked at 130 °C for 15 min in air. Then, the coated substrates were transferred to a N_2-filled glove box. For devices with TFB or PVK single HTLs, TFB solution (10 mg mL^{-1} in chlorobenzene) or PVK solution (10 mg mL^{-1} in chlorobenzene) was spin-coated onto the PEDOT:PSS layer at 3000 rpm for 45 s, followed by baking at 120 °C for 20 min. For devices with a TFB/PVK double HTL, TFB solution (10 mg mL^{-1} in chlorobenzene) was spin-coated at 3000 rpm for 45 s, followed by baking at 120 °C for 20 min. Then PVK solution (2 mg mL^{-1} in 1,4-dioxane) was spin-cast onto the TFB layer at 4000 rpm for 45 s, followed by annealing at 120 °C for 20 min. The $FAPb_{0.7}Sn_{0.3}Br_3$ NCS solution was directly spin-coated at 1500 rpm for 45 s as the emitting layer. Finally, TPBi (40 nm), LiF (1 nm), and aluminum (150 nm) were thermally deposited onto the NC emitting layer under 6×10^{-4} Pa and the devices were encapsulated using a cover glass and a UV-curable epoxy.

Characterization

The thicknesses of the functional layer were measured by using a Bruker DektakXT Stylus Profiler. The absorption spectra were tested by using a UV-violet spectrometer of Beijing Spectrum Analysis 1901 Series at room temperature. A cross-sectional scanning electron microscopy image was obtained by F30 transmission electron microscopy. The PL lifetime decays and steady photoluminescence (PL) were measured by using an Edinburgh Instruments FS5 spectrofluorometer. The surface morphologies were characterized *via* atomic force microscopy (AFM, Asylum Research MFP-3D). The current density–voltage (*J–V*) characteristics were recorded by using a programmable source meter (Keithley 2614B). The forward direction photons emitted from the devices were detected by using a calibrated UDT PIN-25D silicon photodiode.

Conflicts of interest

There are no conflicts to declare.

Acknowledgements

We would like to acknowledge support from the Shenzhen Science and Technology Program (KQTD20170810105439418, KQTD2016030111203005, and JCYJ20170818091233245), the Department of Education of Guangdong Province (2016 KZDXM005), Guangdong Province's Key R&D Program (2019B010925001), the Ministry of Science and Technology of China (2016YFB0401702), and the National Natural Science Foundation of China (61674074 and 61805004).

References

1 L. Protesescu, S. Yakunin, M. I. Bodnarchuk, F. Krieg, R. Caputo, C. H. Hendon, R. X. Yang, A. Walsh and M. V. Kovalenko, *Nano Lett.*, 2015, **15**, 3692–3696.
2 V. K. Ravi, G. B. Markad and A. Nag, *ACS Energy Lett.*, 2016, **1**, 665–671.
3 M. Lu, Y. Zhang, S. Wang, J. Guo, W. W. Yu and A. L. Rogach, *Adv. Funct. Mater.*, 2019, **29**, 1902008.
4 Z. K. Tan, R. S. Moghaddam, M. L. Lai, P. Docampo, R. Higler, F. Deschler, M. Price, A. Sadhanala, L. M. Pazos, D. Credgington, F. Hanusch, T. Bein, H. J. Snaith and R. H. Friend, *Nat. Nanotechnol.*, 2014, **9**, 687–692.
5 A. Sadhanala, S. Ahmad, B. Zhao, N. Giesbrecht, P. M. Pearce, F. Deschler, R. L. Hoye, K. C. Godel, T. Bein, P. Docampo, S. E. Dutton, M. F. De Volder and R. H. Friend, *Nano Lett.*, 2015, **15**, 6095–6101.
6 J. Pan, L. N. Quan, Y. Zhao, W. Peng, B. Murali, S. P. Sarmah, M. Yuan, L. Sinatra, N. M. Alyami, J. Liu, E. Yassitepe, Z. Yang, O. Voznyy, R. Comin, M. N. Hedhili, O. F. Mohammed, Z. H. Lu, D. H. Kim, E. H. Sargent and O. M. Bakr, *Adv. Mater.*, 2016, **28**, 8718–8725.
7 G. Li, J. Huang, H. Zhu, Y. Li, J. X. Tang and Y. Jiang, *Chem. Mater.*, 2018, **30**, 6099–6107.
8 J. S. Yao, J. Ge, B. N. Han, K. H. Wang, H. B. Yao, H. L. Yu, J. H. Li, B. S. Zhu, J. Z. Song, C. Chen, Q. Zhang, H. B. Zeng, Y. Luo and S. H. Yu, *J. Am. Chem. Soc.*, 2018, **140**, 3626–3634.
9 M. Lu, X. Zhang, Y. Zhang, J. Guo, X. Shen, W. W. Yu and A. L. Rogach, *Adv. Mater.*, 2018, **30**, 1804691.
10 H. C. Wang, W. Wang, A. C. Tang, H. Y. Tsai, Z. Bao, T. Ihara, N. Yarita, H. Tahara, Y. Kanemitsu, S. Chen and R. S. Liu, *Angew. Chem., Int. Ed.*, 2017, **129**, 13838–13842.
11 X. Zhang, H. Lin, H. Huang, C. Reckmeier, Y. Zhang, W. C. H. Choy and A. L. Rogach, *Nano Lett.*, 2016, **16**, 1415–1420.
12 Q. W. Liu, S. Yuan, S. Q. Sun, W. Luo, Y. J. Zhang, L. S. Liao and M.-K. Fung, *J. Mater. Chem. C*, 2019, **7**, 4344–4349.
13 K. Lin, J. Xing, L. N. Quan, F. P. G. de Arquer, X. Gong, J. Lu, L. Xie, W. Zhao, D. Zhang, C. Yan, W. Li, X. Liu, Y. Lu, J. Kirman, E. H. Sargent, Q. Xiong and Z. Wei, *Nature*, 2018, **562**, 245–248.
14 T. Chiba, Y. Hayashi, H. Ebe, K. Hoshi, J. Sato, S. Sato, Y. J. Pu, S. Ohisa and J. Kido, *Nat. Photonics*, 2018, **12**, 681–687.
15 L. Lan, B. Liu, H. Tao, J. Zou, C. Jiang, M. Xu, L. Wang, J. Peng and Y. Cao, *J. Mater. Chem. C*, 2019, **7**, 5755–5763.
16 M. Auer-Berger, R. Trattnig, T. Qin, R. Schlesinger, M. V. Nardi, G. Ligorio, C. Christodoulou, N. Koch, M. Baumgarten, K. Müllen and E. J. W. List-Kratochvil, *Org. Electron.*, 2016, **35**, 164–170.

17 Y. Zou, M. Ban, Y. Yang, S. Bai, C. Wu, Y. Han, T. Wu, Y. Tan, Q. Huang, X. Gao, T. Song, Q. Zhang and B. Sun, *ACS Appl. Mater. Interfaces*, 2018, **10**, 24320–24326.
18 X. Liang, S. Bai, X. Wang, X. Dai, F. Gao, B. Sun, Z. Ning, Z. Ye and Y. Jin, *Chem. Soc. Rev.*, 2017, **46**, 1730–1759.
19 L. Zhang, X. Yang, Q. Jiang, P. Wang, Z. Yin, X. Zhang, H. Tan, Y. Yang, M. Wei, B. R. Sutherland, E. H. Sargent and J. You, *Nat. Commun.*, 2017, **8**, 15640.
20 H. Wu, Y. Zhang, X. Zhang, M. Lu, C. Sun, T. Zhang and W. W. Yu, *Adv. Opt. Mater.*, 2017, **5**, 1700377.
21 X. Zhang, C. Sun, Y. Zhang, H. Wu, C. Ji, Y. Chuai, P. Wang, S. Wen, C. Zhang and W. W. Yu, *J. Phys. Chem. Lett.*, 2016, **7**, 4602–4610.
22 X. Dai, Z. Zhang, Y. Jin, Y. Niu, H. Cao, X. Liang, L. Chen, J. Wang and X. Peng, *Nature*, 2014, **515**, 96–99.
23 Y. Liu, C. Jiang, C. Song, J. Wang, L. Mu, Z. He, Z. Zhong, Y. Cun, C. Mai, J. Wang, J. Peng and Y. Cao, *ACS Nano*, 2018, **12**, 1564–1570.
24 L. Zheng, G. Zhai, Y. Zhang, X. Jin, L. Gao, Z. Yun, Y. Miao, H. Wang, Y. Wu and B. Xu, *Superlattices Microstruct.*, 2020, **140**, 106460.
25 C. Wu, T. Wu, Y. Yang, J. A. McLeod, Y. Wang, Y. Zou, T. Zhai, J. Li, M. Ban, T. Song, X. Gao, S. Duhm, H. Sirringhaus and B. Sun, *ACS Nano*, 2019, **13**, 1645–1654.
26 R. Li, L. Cai, Y. Zou, H. Xu, Y. Tan, Y. Wang, J. Li, X. Wang, Y. Li, Y. Qin, D. Liang, T. Song and B. Sun, *ACS Appl. Mater. Interfaces*, 2020, **12**, 36681–36687.
27 C. Zou, Y. Liu, D. S. Ginger and L. Y. Lin, *ACS Nano*, 2020, **14**, 6076–6086.
28 Y. Liu, J. Cui, K. Du, H. Tian, Z. He, Q. Zhou, Z. Yang, Y. Deng, D. Chen, X. Zuo, Y. Ren, L. Wang, H. Zhu, B. Zhao, D. Di, J. Wang, R. H. Friend and Y. Jin, *Nat. Photonics*, 2019, **13**, 760–764.
29 H. Chen, K. Ding, L. Fan, W. Liu, R. Zhang, S. Xiang, Q. Zhang and L. Wang, *ACS Appl. Mater. Interfaces*, 2018, **10**, 29076–29082.
30 Z. Gao, C. S. Lee, I. Bello, S. T. Lee, R. M. Chen, T. Y. Luh, J. Shi and C. W. Tang, *Appl. Phys. Lett.*, 1999, **74**, 865–867.
31 R. Cai, X. Qu, H. Liu, H. Yang, K. Wang and X. W. Sun, *IEEE Trans. Nanotechnol.*, 2019, **18**, 1050–1056.
32 D. Han, M. Imran, M. Zhang, S. Chang, X. Wu, X. Zhang, J. Tang, M. Wang, S. Ali, X. Li, G. Yu, J. Han, L. Wang, B. Zou and H. Zhong, *ACS Nano*, 2018, **12**, 8808–8816.
33 M. K. Gangishetty, S. Hou, Q. Quan and D. N. Congreve, *Adv. Mater.*, 2018, **30**, 1706226.
34 J. R. Manders, S. W. Tsang, M. J. Hartel, T. H. Lai, S. Chen, C. M. Amb, J. R. Reynolds and F. So, *Adv. Funct. Mater.*, 2013, **23**, 2993–3001.
35 S. Liu, R. Liu, Y. Chen, S. Ho, J. H. Kim and F. So, *Chem. Mater.*, 2014, **26**, 4528–4534.